Arrested Foveal Development in Preterm Eyes: Thickening of the Outer Nuclear Layer and Structural Redistribution Within the Fovea

Johan Sjöstrand,[1] Rebecka Rosén,[2] Maria Nilsson,[2] and Zoran Popovic[1]

[1]Department of Ophthalmology, University of Gothenburg, Gothenburg, Sweden
[2]Unit of Optometry, Department of Clinical Neuroscience, Karolinska, Stockholm, Sweden

Correspondence: Johan Sjöstrand, Department of Ophthalmology, SU/Mölndal, 43180 Mölndal, Sweden; johan.sjostrand@oft.gu.se.

Submitted: June 1, 2017
Accepted: August 16, 2017

Citation: Sjöstrand J, Rosén R, Nilsson M, Popovic Z. Arrested foveal development in preterm eyes: thickening of the outer nuclear layer and structural redistribution within the fovea. *Invest Ophthalmol Vis Sci*. 2017;58:4948–4958. DOI:10.1167/iovs.17-22333

Purpose. The aim of this study was to define landmarks to better characterize foveal microstructure in normal subjects and in preterms with or without signs of immaturity, and to report on thickness changes of outer foveal layers following analysis of optical coherence tomography (OCT) B-scan images.

Methods. Selected eyes from eight young adults with a history of prematurity (24–33 weeks of gestation) and five controls were imaged using conventional and directional OCT. Retinal layer thickness analysis was performed at selected temporal eccentricities defined by the individual distance between two landmarks for each case, the foveal center and the foveal rim.

Results. The use of a foveal center and foveal rim landmark transformation enabled comparisons of interindividual B-scans at corresponding landmark positions in both controls and preterms. We found a 20% shorter foveal center to foveal rim distance in preterms with an immature fovea than in controls. Reflectometric and manual segmentation measurements showed increased thickness of inner retinal layers and photoreceptor cell body and outer plexiform layers centrally, but no observable change of photoreceptor inner and outer segment thickness.

Conclusions. Our landmark-based analysis of OCT images using reflectometry and manual segmentation provides complementary findings in comparisons of normal and immature foveal structures. We show a central thickness increase in the outer nuclear layer, outer plexiform layer, and postreceptor layers in preterms with signs of arrested foveal development. We found no indication of abnormal photoreceptor inner or outer segment development in preterms.

Keywords: foveal layer topography, foveal landmarks, reflectometric analysis, optical coherence tomography, persisting signs of prematurity

The human fovea is a complex structure formed by migration and transformation of various cell populations during development.[1,2] The marked variability of layer thicknesses between the foveal center and the region with maximal retinal thickness makes averaging of certain regions problematic, as in, for example, the Early Treatment Diabetic Retinopathy Study (ETDRS) grid.[3] Interindividual variability of normal foveal microstructure adds to this complexity.[4–6]

Optical coherence tomography (OCT) is an established imaging technique that enables noninvasive visualization of the normal and abnormal retina.[7,8] Although retinal structures can be characterized using built-in OCT image analysis software, inherent limitations, such as the inability to differentiate adjacent layers due to similar layer reflectance properties or abnormal structural changes, may necessitate the use of other techniques. Longitudinal reflectometric profiles[9–11] have been used to study local features of retinal layers, and directional OCT imaging[12–14] enables the separation of the outer plexiform layer (OPL), Henle fiber layer (HFL), and outer nuclear layer (ONL). Irrespective of the method of choice there is a need for a strategy to select relevant and informative measurement positions to better describe the topography and microstructure of the normal and abnormal fovea.

A starting point for the search of appropriate measurement positions is obviously the definition of possible landmarks of the inner and outer parts of the fovea. Little information is found in the clinical literature defining the adult fovea, and there are no consistent ophthalmoscopic descriptions of landmarks.[15] OCT studies have evaluated foveal pit metrics such as foveal center diameter, foveal slope, and foveal margin,[5] but definitions of other landmarks are lacking. However, Polyak[16] describes possible landmarks in his extensive monograph of the anatomy of the human retina, and Curcio and colleagues[17] give a detailed description of the various layers of the adult fovea. The dynamics and histologic characteristics during normal development of the fovea have also been described.[2,18–20]

A combination of anatomic and OCT image analysis of the developing normal fovea has revealed structural correlates and enabled the interpretation of OCT images in many respects.[21] Analyses of spectral-domain OCT (SD-OCT) images of the fovea before and after full-term birth have shown the dynamic changes in different foveal layers from approximately 30 weeks

Copyright 2017 The Authors

This work is licensed under a Creative Commons Attribution-NonCommercial-NoDerivatives 4.0 International License.

Downloaded from iovs.arvojournals.org on 04/25/2024

Table 1. Demographic Data of Prematurity Groups and Controls

Groups	GA, Weeks	BW, g	SE, Diopters	BCVA, Decimal	AL, mm
PG1*, $n = 3$	28–32	750–1750	+1 to −0.5	1.2–1.6	23.4–24.5
PG2†, $n = 3$	29–33	1170–2100	0 to −13	1.0–1.5	23.9–28.3
PG3‡, $n = 2$	24–26	700–870	−0.5 to −3.5	1.0–1.25	NA
Controls, $n = 5$	NA	NA	+1.25 to −4.75, (median −0.25)	1.0–1.2, (median 1.2)	22.1–25.2, (median 23.0)

All data are presented with range values for PG1 to PG3. Both ranges and medians are given for the control group. GA, gestational age; BW, birth weight; SE, spherical equivalent; BCVA, best-corrected visual acuity; NA, not available.

* PG1, prematurity group 1 (no signs of foveal immaturity and no ROP).

† PG2, prematurity group 2 (incomplete IRL displacement, shallow foveal pit, and no ROP).

‡ PG3, prematurity group 3 (incomplete IRL displacement, very shallow foveal pit, and treated ROP).

of gestation through different stages of normal maturation.[21,22] In general, development follows a timeline with continuous increases in layer thicknesses,[23] but in some preterms with or without retinopathy the development of the inner retina is arrested at a certain stage.[24,25]

In a previous study of preterms born extremely premature we found persisting signs of immaturity indicating retardation of several developmental events when imaged by low-resolution SD-OCT at an age of 6.5 years.[26] One finding of this study was remarkable: The combined thickness of the OPL, HFL, ONL, and inner segment (IS) layer at the foveal center was proportionally increased compared to that at the position of maximal foveal thickness in cases with marked immaturity. Similar observations of a proportional central increase of these outer retinal layers compared to periphery have been reported in previous OCT studies of cases with prematurity or retinopathy of prematurity (ROP).[25,27,28] These interesting observations of structural changes at the foveal center involving the combined photoreceptor cell body and axon layers, and also of true ONL as a separate layer, make it important to further analyze the outer retina in cases with a history of prematurity in spite of observations of unchanged photoreceptor segment layers.[27]

The OPL, HFL, and ONL are difficult to separate due to poor reflectivity differences between these layers in conventional OCT images. However, the introduction of directional OCT[12,14] with analyses of tilted images enables the separation of these layers. Qualitative observations of tilted images in our previous study of preterms indicated increased thickness of the ONL.[26]

The aim of our study was to identify a strategy to characterize the foveal topography and microstructure in normal subjects and in preterms with or without signs of immaturity, such as incomplete displacement of inner retinal layers from the foveal center. We report on landmark definitions and redistribution of the outer foveal layers following analysis of conventional and directional SD-OCT images. Thickening of the photoreceptor cell body and pedicle/synapse layers was observed in the central part of the fovea in addition to the clinically observable changes of the inner postreceptor layers.

Methods

The research followed the tenets of the Declaration of Helsinki. All subjects were informed about the goals, consequences, and protocol of the study and then provided their written informed consent.

Subjects

Selected eyes from eight young adults (four females) with a history of prematurity (24–33 weeks of gestation) and five controls (Table 1) were imaged using two commercial SD-OCT systems (Cirrus HD-OCT 4000 and 5000; Carl Zeiss Meditec, Dublin, CA, USA) at the Optometry Clinic, Karolinska Institutet, Stockholm, Sweden.

The preterms, 22 to 33 years of age at examination, were divided into three subgroups based on the degree of foveal immaturity after clinical grading of OCT scans at the foveal center (FC) (Table 1). The degree of foveal immaturity was based on signs of reduced foveal depth (FD) and presence of postreceptor or inner retinal layers (IRL) at FC. The preterm groups (PG) were classified as follows: PG1 ($n = 3$), no signs of foveal immaturity; PG2 ($n = 3$) and PG3 ($n = 2$), incomplete displacement of IRL and reduced FD indicating arrested foveal development. In PG1 and PG2 none of the subjects had history of ROP, while both subjects in PG3 had received cryotherapy treatment due to ROP. Axial length (AL) was not available in the two PG3 subjects.

In addition, five control subjects (all females) aged 20 to 33 years were recruited among staff members and students at the Optometry School at Karolinska Institutet, Stockholm, Sweden. Inclusion criteria were birth at term, no history of ocular disease, and absence of visual complaint.

OCT Imaging and Analysis

Centered and displaced SD-OCT entrance beam positions were used to obtain straight and tilted scans, respectively, with the Cirrus HD-OCT from Zeiss. All high-definition images were captured using the HD 5 Line Raster protocol without spacing between scans, and each B-scan was imaged 20 times. Straight scans (i.e., horizontal SD-OCT B-scans with entrance beam positions through the pupil center with a distinct light reflex in the foveal pit) were selected for reflectometric analysis. These images showed most marked differences between hyperreflective and hyporeflective layers and best defined borders between retinal layers of interest compared to tilted scans obtained with OCT entrance beam positions displaced from the pupil center. The displacement from the pupil center was individually adjusted to obtain maximum hyperreflectivity of the HFL over the imaging area. Straight scans and tilted scans, with entrance beam positions displaced from the pupil center, were selected for manual segmentation of outer retinal layers (OPL, HFL, and ONL).

All images were registered, averaged, and flattened to the posterior retinal pigment epithelium (RPE) boundary using a two-step procedure. Image preprocessing was performed using software in the public domain (Fiji 1.48v)[29] and included cropping images to same size, grouping images in a stack, registering the image stack using scaled rotation, and creating an average image from the registered stack. Average images were flattened using semiautomatic custom software written in MATLAB (2014a; Mathworks, Natick, MA, USA) that is freely available upon request:

1. Images were oversampled by a factor of 4 to avoid edge artifacts during flattening.
2. Points along the posterior boundary of the RPE layer were selected manually.

Investigative Ophthalmology & Visual Science

Downloaded from iovs.arvojournals.org on 04/25/2024

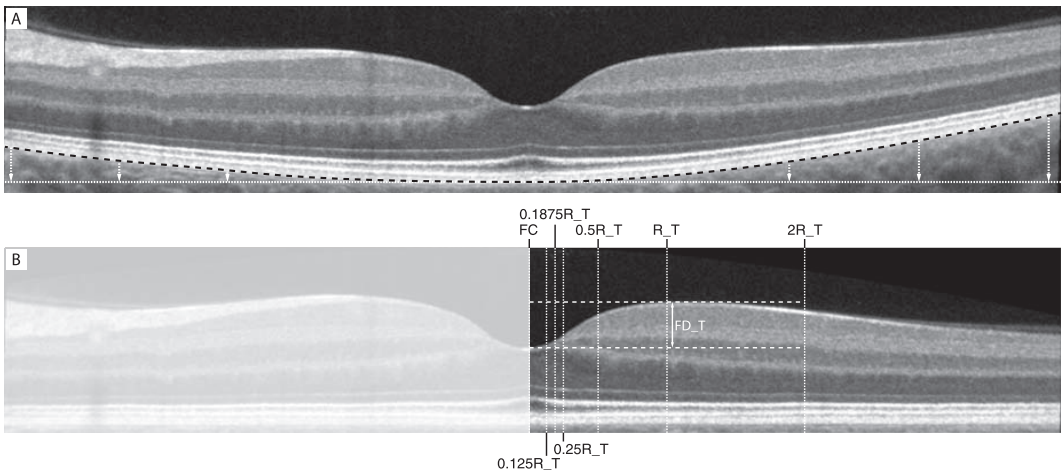

FIGURE 1. (**A**) Registered average of straight SD-OCT B-scan image of normal retina (C-1). *Black dashed line* indicates polynomial fit to RPE layer, and *white dotted line* indicates horizontal tangent to the minimum of the fitted polynomial. *Arrows* indicate vertical straightening translation. (**B**) Image of normal retina in (**A**) after flattening to the RPE layer. *White vertical lines* indicate measurement positions along the temporal (T) hemimeridian, which was selected for analysis to avoid the thicker nerve fiber layer on the nasal side. The R position was defined by the intersection of the *upper dashed horizontal line* and the ILM (only temporal side shown). The *lower dashed horizontal line tangential* indicates the bottom of the foveal pit. Foveal depth (FD) was defined as the difference between the average of nasal and temporal retinal thickness at R and retinal thickness at FC (only FD_T shown). FC, foveal center; R, foveal rim; 0.125R, 1/8 of R; 0.1875R, 3/16 of R; 0.25R, 1/4 of R; 0.5R, 1/2 of R; 2R, double foveal rim distance.

3. A polynomial was fit to the identified points (Fig. 1A).
4. Images were flattened by sliding each image column vertically downward to align all polynomial pixels to a horizontal line defined by the minimum of the fitted polynomial (Fig. 1A).
5. Flattened images (Fig. 1B) were downsampled to original size and saved for subsequent analysis.

All image analysis was performed using Fiji 1.48v. The temporal side was selected for analysis to avoid the asymmetry caused by the marked thickening of the retinal nerve fiber layer (RNFL) on the nasal side in SD-OCT B-scan images (Fig. 1B). The *x*-coordinates of the FC and foveal rim (R) positions were identified in the flattened images. The FC position in the flattened images was defined as the maximum ±3 pixels of the outer segment (OS) bulge (inner segment/outer segment [IS/OS] line) based on peak quality of the longitudinal reflectometric profile. The R position was defined as the first pixel where the inner limiting membrane (ILM) of the foveal slope intersects a horizontal line tangential to the ILM. This was accomplished in Fiji by vertically displacing a horizontal line, parallel to the RPE in the flattened image, until it intersected the ILM (Fig. 1B). Foveal depth was defined as the difference between the average of nasal and temporal retinal thickness at R and retinal thickness at FC (Fig. 1B) in the flattened images.

Longitudinal reflectometric profiles were obtained at FC and six temporal positions displaced 12.5% (0.125R), 18.75% (0.1875R), 25% (0.25R), 50% (0.5R), 100% (R), and 200% (2R) of the foveal rim distance from FC along the temporal hemimeridian in flattened straight images (Fig. 2). Manual segmentation was performed at FC, 0.25R, 0.5R, R, and 2R positions in flattened straight and tilted images.

The temporal rim position of one case (PG3-2) was estimated from the nasal rim position due to a very flat temporal thickness profile. Analysis by reflectometry and manual segmentation of conventional OCT B-scan images was possible in all cases, whereas directional OCT B-scan images could not be obtained for the two PG3 cases. Mean ± SD retinal layer thicknesses were calculated from measurements of peak-to-peak distances in longitudinal reflectometric profiles or manually segmented borders (Fig. 3).

The scan length of an OCT differs between subjects due to interindividual variations in AL. Individual retinal scaling factors[30] calculated from AL measurements were used to compensate for these differences in lateral magnification in all groups except the PG3 group, where AL was not measured. Retinal scaling factors (mean ± SD) were 0.95 ± 0.06 for controls, 0.98 ± 0.02 for PG1, and 1.05 ± 0.10 for PG2. The calibrated value of 24.46 mm of the Cirrus SD-OCT, yielding a retinal scaling factor of unity, was used for the two PG3 cases.

Images for manual segmentation were obtained using both conventional and directional OCT. By horizontally varying the OCT entry position over the pupil of the eye to an off-axis position relative to position of the conventional scan, directional OCT yields tilted images with a hyperreflective HFL relative to the ONL on the tilt-down side and a hyporeflective HFL relative to the ONL on the tilt-up side (Fig. 4). This method enables direct visualization and quantification of OPL, HFL, and ONL thickness.

RESULTS

Quantitative evaluation of the normal/abnormal central fovea based on measurements of FD and IRL from the ILM to the inner nuclear layer (INL) covering FC (Fig. 5) confirmed the clinical grading (cf. Methods). Marked changes in FD and IRL displacement at FC were observed in PG2 and PG3 compared to controls and PG1 cases and were defined as signs of arrested foveal development.

The foveal pit minimum position was displaced temporally relative to the OS bulge maximum position in all but three subjects, with nasal displacement in two subjects and coincident in one subject (Table 2). It is notable that a displacement greater than 25 μm was found in two controls and the majority (4/5) of PG2 and PG3 cases.

The profile of the central fovea (FC to 0.25R) was changed in the two groups of preterms with abnormal central retina (PG2 and PG3) with increased thickness of postreceptor layers (IRL), pedicle/synapse layer (OPL), and photoreceptor cell body (ONL) layer (Figs. 6, 7).

Downloaded from iovs.arvojournals.org on 04/25/2024

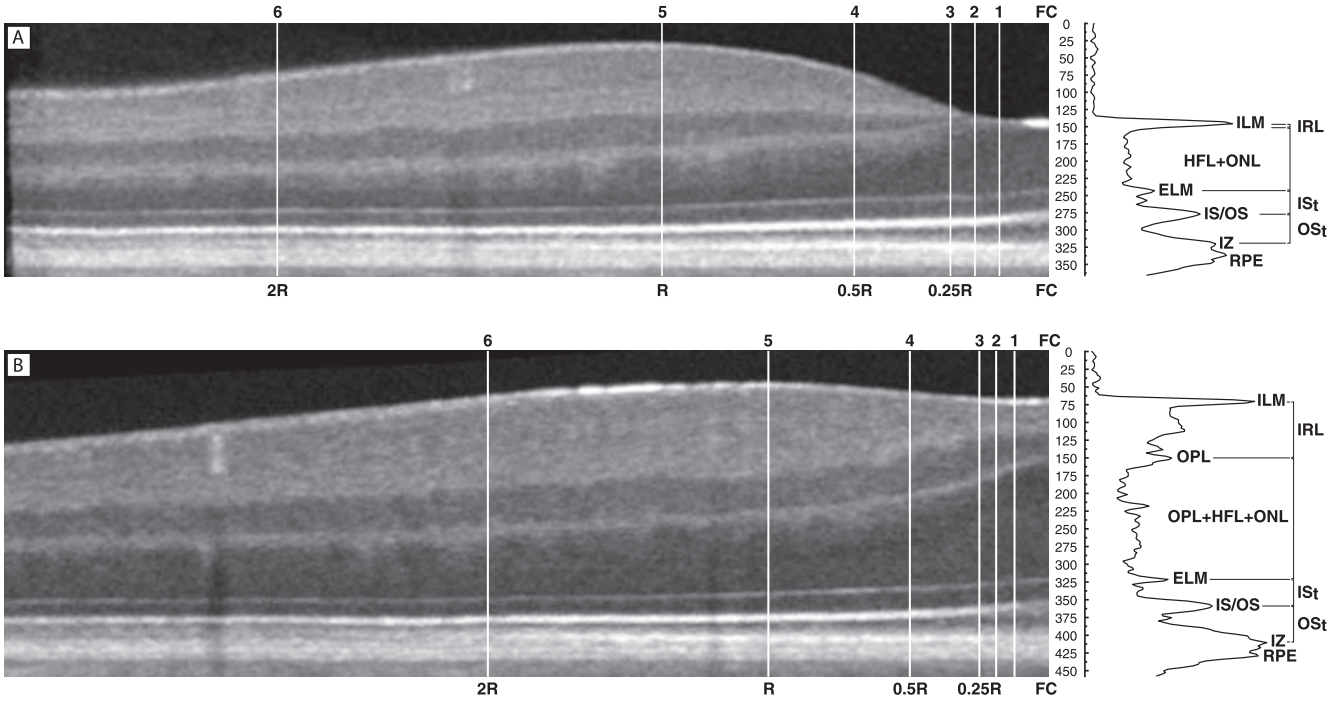

Figure 2. Straight SD-OCT images of temporal (**A**) normal (C-3) and (**B**) preterm (PG3-1) retina after flattening to the RPE layer. *White vertical lines* indicate measurement positions defined by the foveal center (FC) and foveal rim (R) distance. Mean ± SD retinal layer thicknesses were calculated from measurements of peak-to-peak distances in the longitudinal reflectometric profiles (*top and bottom right*). FC, foveal center; 1, 0.125R; 2, 0.1875R; 3, 0.25R; 4, 0.5R; 5, R; 6, 2R; ILM, inner limiting membrane; IRL, inner retinal layers; OPL, outer plexiform layer; HFL, Henle fiber layer; ONL, outer nuclear layer; ELM, external limiting membrane; ISt, inner segment layer thickness; IS/OS, inner segment outer segment junction line; OSt, outer segment layer thickness; IZ, interdigitation zone; RPE, retinal pigment epithelium layer.

The difference in layer thickness at the foveal rim between controls and preterms was small, with the exception of case PG3-1, whose data were outside the range of the others.

The temporal rim (R) position varied in controls between 810 and 1050 μm with a trend toward more central positions in PG2 and PG3 (Table 2). Due to this variability, the measurement position eccentricities for controls and preterms were expressed as a percentage of the temporal rim position in comparisons of reflectometric data (Fig. 6) and as a mean micrometer scale for manually segmented data (Figs. 7, 8).

In a search for landmarks besides FC and R, we also studied the location of the central edge of the OPL (i.e., the most central position where the OPL band, or inner portion of the OPL according to the histologic definition,[16] first appeared). The OPL band could not be found at FC in controls (Fig. 2A), and first appearance was noted at eccentricities ranging from 135 to 225 μm or approximately one-fifth of the FC to R distance. In PG1, with complete central IRL displacement, the central edge of the OPL was located more centrally (at 82–102 μm eccentricity) in two out of three cases (Table 2). The position of the central edge of the OPL was also an indicator of the appearance of the IRL below the ILM in the control and PG1 groups. An OPL band covered FC in all cases with arrested foveal development (PG2 and PG3 groups) (Fig. 2B) at a relative depth from the ILM ranging from 10% in PG2 to 26% in PG3 of the total retinal thickness at FC (Fig. 5).

Reflectivity profiles of the outer retina showed three highly reflective photoreceptor bands representing the external limiting membrane (ELM) (peak 1), the junction of the photoreceptor inner and outer segments (IS/OS) (peak 2), and the interdigitation zone (IZ) (peak 3) both in controls and in preterms at all measurement positions. In general, peaks 1 to 3 were well-defined single peaks, whereas the RPE band was sometimes divided into two or more peaks. In a few cases, where peaks 1 to 3 were vaguely defined, a new longitudinal reflectometric profile was acquired at a lateral position 1 to 5 pixels away to ensure a clear definition of the peaks.

Distance measurements between peaks 1 to 3 could be performed on single well-defined peaks. Only scattered values were obtained of the RPE thickness (the distance between peak 3 and 4) due to complexity of the RPE peak.

The IS/OS was less reflective than the IZ for all cases at FC, but this difference decreased with increasing eccentricity due to a marked increase in IS/OS intensity relative to the other.[31]

The mean thickness of the combined OPL + HFL + ONL in controls was 100 μm at FC and increased to a plateau of 120 μm at 0.1875R (approximately 200 μm eccentricity) (Fig. 6B). The OPL + HFL + ONL profile from FC to 0.25R was markedly changed in all cases with shallow foveal depression and incomplete central IRL displacement. The combined OPL + HFL + ONL mean thickness was increased at FC (130 μm in PG2 and 159 μm in PG3 compared to 100 and 102 μm in controls and PG1, respectively) and showed a centrally displaced position of maximal thickness compared to controls (Fig. 6B). The contribution of increased OPL + HFL + ONL thickness to increased total retinal thickness was 60% in PG2 and 43% in PG3.

In contrast, the OS profile showed small differences between controls and preterms (Fig. 6B). A central lengthening of photoreceptor OS was noted in all cases with a decline of approximately 20 μm between FC and 2R (Fig. 6B). The decline was steeper centrally, approximately 10 μm from FC to 0.25R, followed by a more gradual decline from 0.25R to 2R.

The thickness of IS and OS layers at FC of controls and prematurity groups was within the same range (Fig. 6B). IS thickness showed small changes with eccentricity from FC to 0.5R, and thus the profile of the combined IS/OS layer was almost parallel to that of OS alone (Fig. 6B).

Investigative Ophthalmology & Visual Science

Downloaded from iovs.arvojournals.org on 04/25/2024

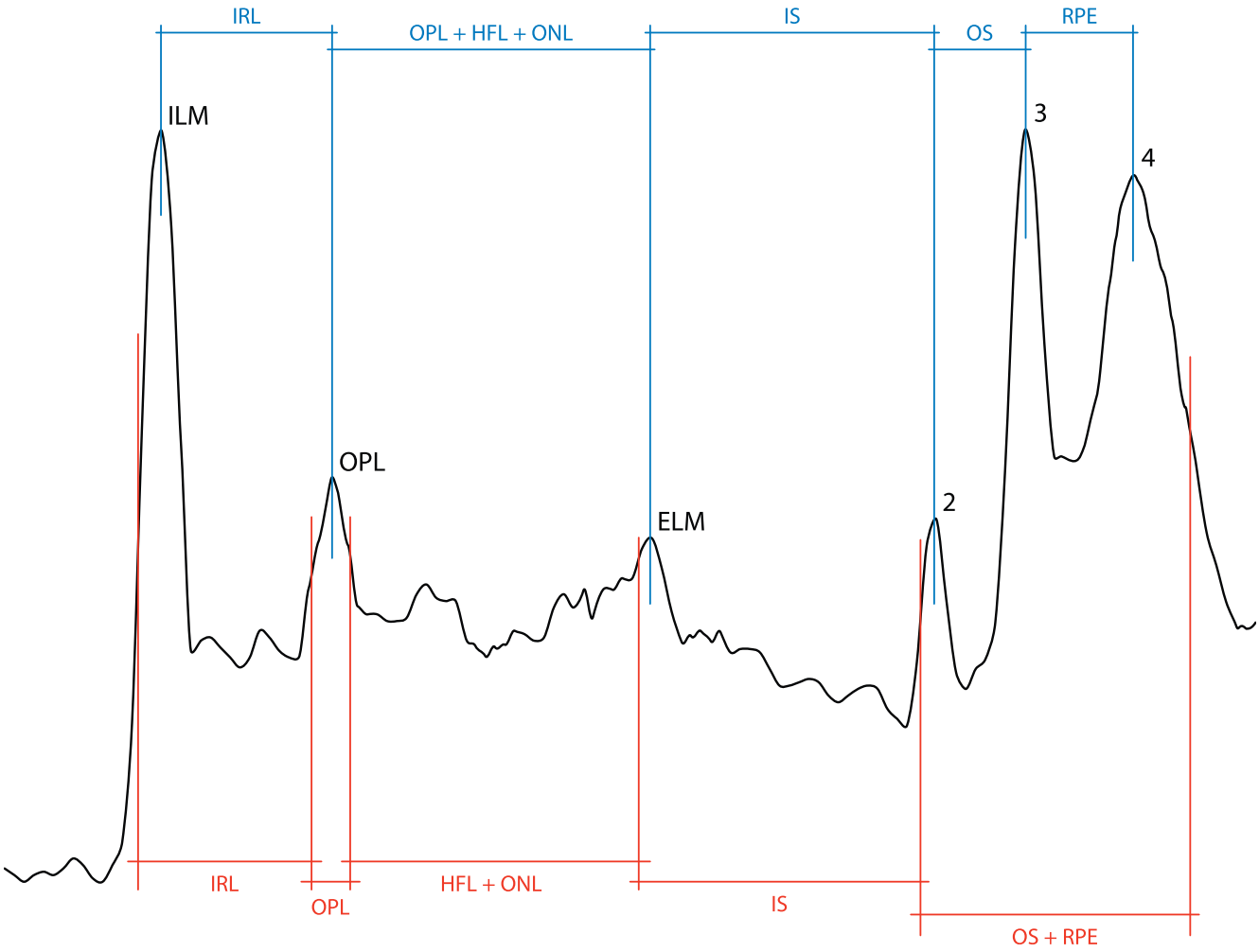

Figure 3. Schematic of layer thickness definitions used for reflectometric (*blue*, *top*) and manual (*red*, *bottom*) measurements.

Whereas reflectometric analysis was more precise for separate measurements of photoreceptor segment layers, manual segmentation of images from conventional and directional OCT revealed the separate profiles of the OPL, HFL, and ONL. Measurements of the ONL and hyporeflective HFL on the tilt-up side were chosen for measurements outside the foveola (0.25R), whereas analyses of the foveola were performed on conventional images.

We found increased thickness of the separate OPL and ONL at FC for PG2 compared to controls (Fig. 7). The most marked changes were seen in the pedicle/synapse (OPL) and the photoreceptor cell body (ONL) layers whereas the change of HFL was marginal (overlapping error bars) and limited to FC. Compared to controls, true ONL represented 57% (21 μm) and 47% (32 μm) of the total increase of the combined OPL + HFL + ONL at FC in PG2 and PG3, respectively. No increase was found for ONL in PG1. Cumulative thickness changes due to individual thickening of OPL, HFL, and ONL in PG2 compared to controls are shown in Figure 8. Analysis of layer thickening contributing to a shallow fovea showed that an increase of the OPL and ONL was evident within the central 200 μm with smaller differences toward the foveal rim.

Discussion

In prematurity group PG1 with normal FD and complete displacement of IRL from FC, the foveal characteristics were

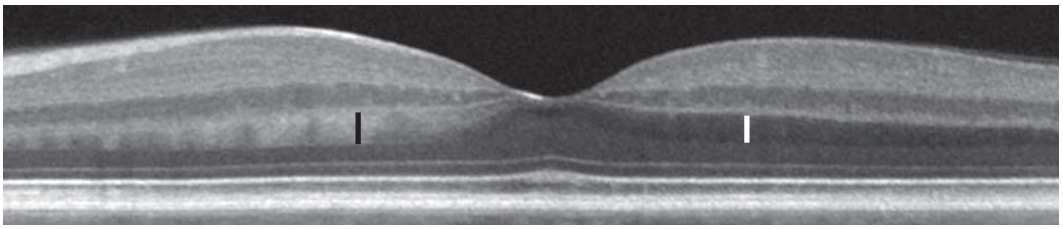

Figure 4. Flattened directional OCT image of subject PG1-1 displaying a foveal microstructure similar to that of controls. The HFL is hyperreflective as indicated in part by the *black rectangle* on the nasal (*left*) side and hyporeflective as indicated in part by the *white rectangle* on the temporal (*right*) side. Measurement from the side with a hyporeflective HFL is presented in this study.

Investigative Ophthalmology & Visual Science

Downloaded from iovs.arvojournals.org on 04/25/2024

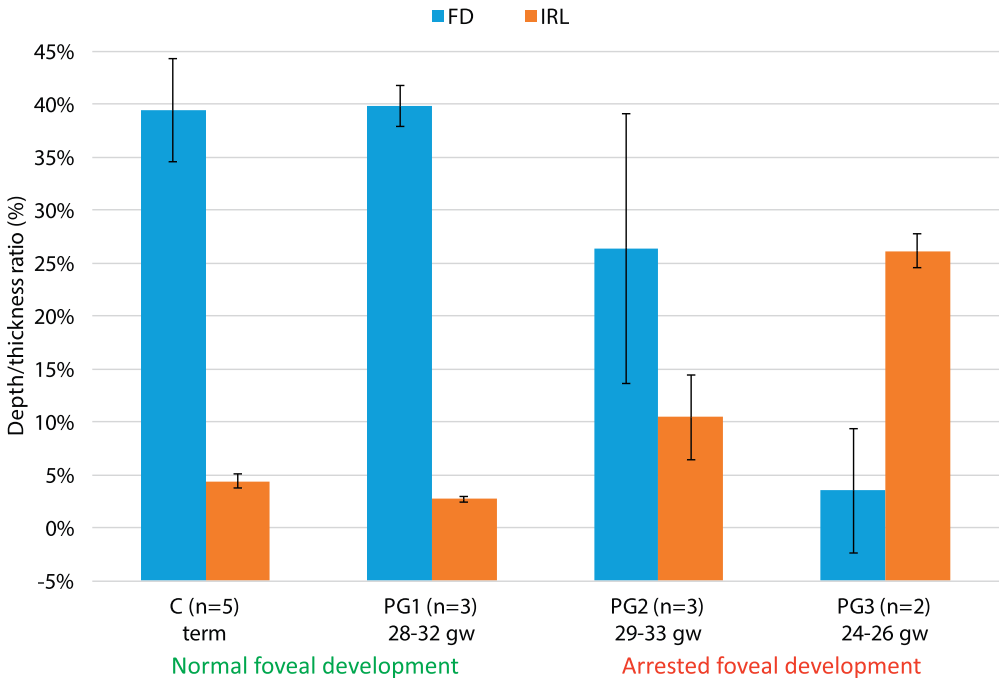

Figure 5. Percentage ratios (mean ± SD) of FD (ratio of FD at FC and total retinal thickness at R) and of IRL displacement (ratio of IRL thickness at FC and total retinal thickness at FC) of controls (C) and premature groups (PG1, PG2, and PG3).

within normal limits. In the other two prematurity groups (PG2 and PG3), all cases were selected to have signs of arrested foveal development (i.e., incomplete displacement of IRL from FC and reduced FD as observed in previous studies of preterms).[24,26–28,32,33] The central part of the normal mature fovea out to approximately 200 μm is thus characterized by the lack of an OPL and a slightly curved foveal floor. This central zone also corresponds to an area of the outer part of the retina characterized by an OS bulge caused by a lengthening of photoreceptor OS as reported in studies based on histologic characteristics.[16,17,34] The major changes observed in preterms with arrested foveal development in the present study occur in this central zone, that is, the foveola.

The most central position where the photoreceptors connect to the postreceptor retinal layers via cone pedicles and synapses is a very interesting structural feature. The detectability by reflectometry of this position of the central OPL edge gives us a tool in analyzing OCT images to estimate the most central connection between inner and outer foveal structures. Comparison between structural features from anatomy and OCT images have indicated that OPL is the structural correlate to the layer with cone pedicles and synapses connecting the photoreceptors to the IRL.[17] The position of the central edge of the OPL at approximately 200 μm is in agreement with the observation of lack of cone pedicles from FC out to 100 μm[35,36] and the appearance of a continuous layer of pedicles at the border of the foveola.[16,20,35] This edge position in OCT images of controls at approximately 20% of the foveal rim distance from FC also indicates the start of the foveal slope with the appearance and increasing

Table 2. Magnitude and Direction of Displacement of Foveal Pit Minimum Position From OS Bulge Maximum Position, First Appearance of the Central OPL Edge, and Rim Position Along the Temporal Hemi-Meridian in Control (C) and Premature (PG) Subjects

	Foveal Pit/OS Bulge Displacement		Central OPL Edge*		R_T Position	
Subjects	μm	Direction	μm	% of Mean C	μm	% of Mean C
C-1	7	N	174	91	810	84
C-2	17	T	221	116	1018	106
C-3	27	T	225	118	1050	109
C-4	13	T	135	71	934	97
C-5	35	T	196	103	1011	105
PG1-1	34	T	102	54	1028	107
PG1-2	20	T	82	43	982	102
PG1-3	0	None	228	120	861	89
PG2-1	6	T	Incomplete displacement, OPL covers FC		661	69
PG2-2	30	N			866	90
PG2-3	57	T			697	72
PG3-1	75	T	Incomplete displacement, OPL covers FC		793	82
PG3-2	134	T			503	52

N, nasal; T, temporal.
* Detected in reflectometric scans below the highly reflective ILM in control and PG1 subjects.

Investigative Ophthalmology & Visual Science

Downloaded from iovs.arvojournals.org on 04/25/2024

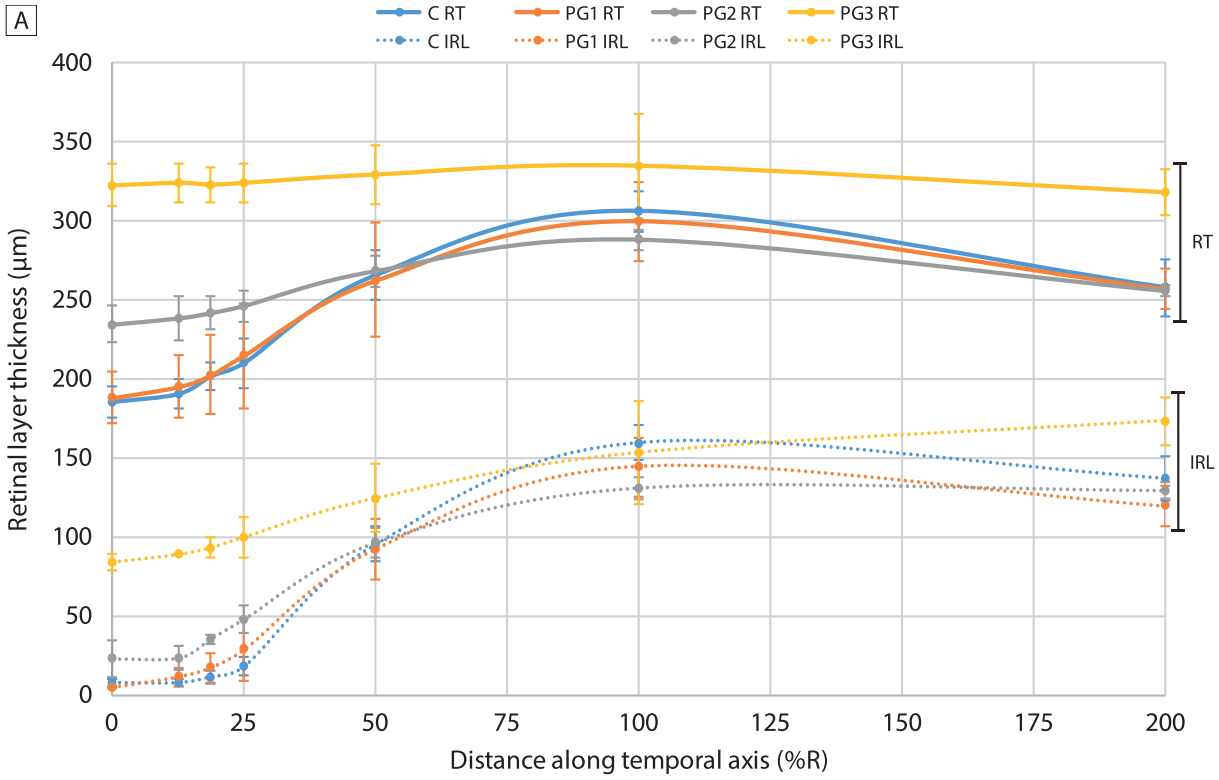

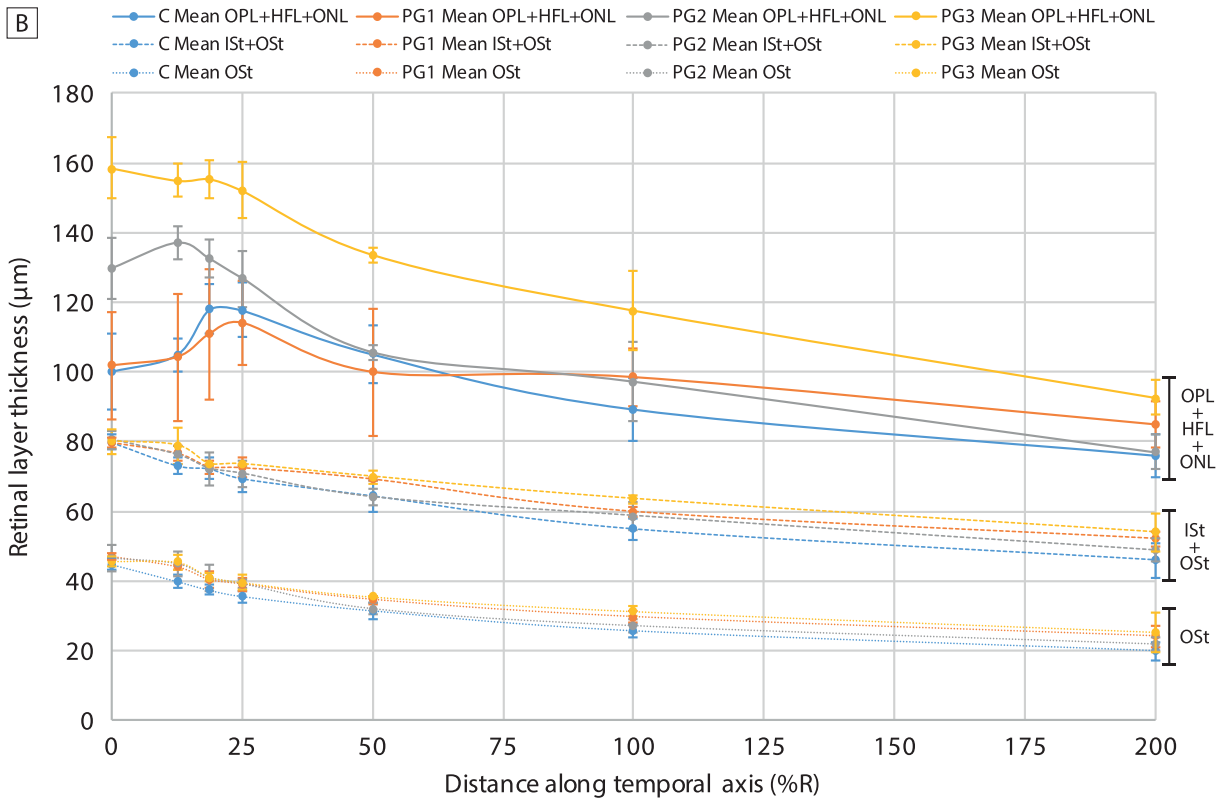

Figure 6. Longitudinal reflectometric profile measurements of retinal layer thickness in micrometers (mean ± SD) of (**A**) RT and IRL and (**B**) OPL + HFL + ONL, ISt + OSt, and OSt along the temporal axis of control (C) and premature groups. Distance along the temporal axis is specified in percent of the foveal rim (R) distance from FC.

Investigative Ophthalmology & Visual Science

Downloaded from iovs.arvojournals.org on 04/25/2024

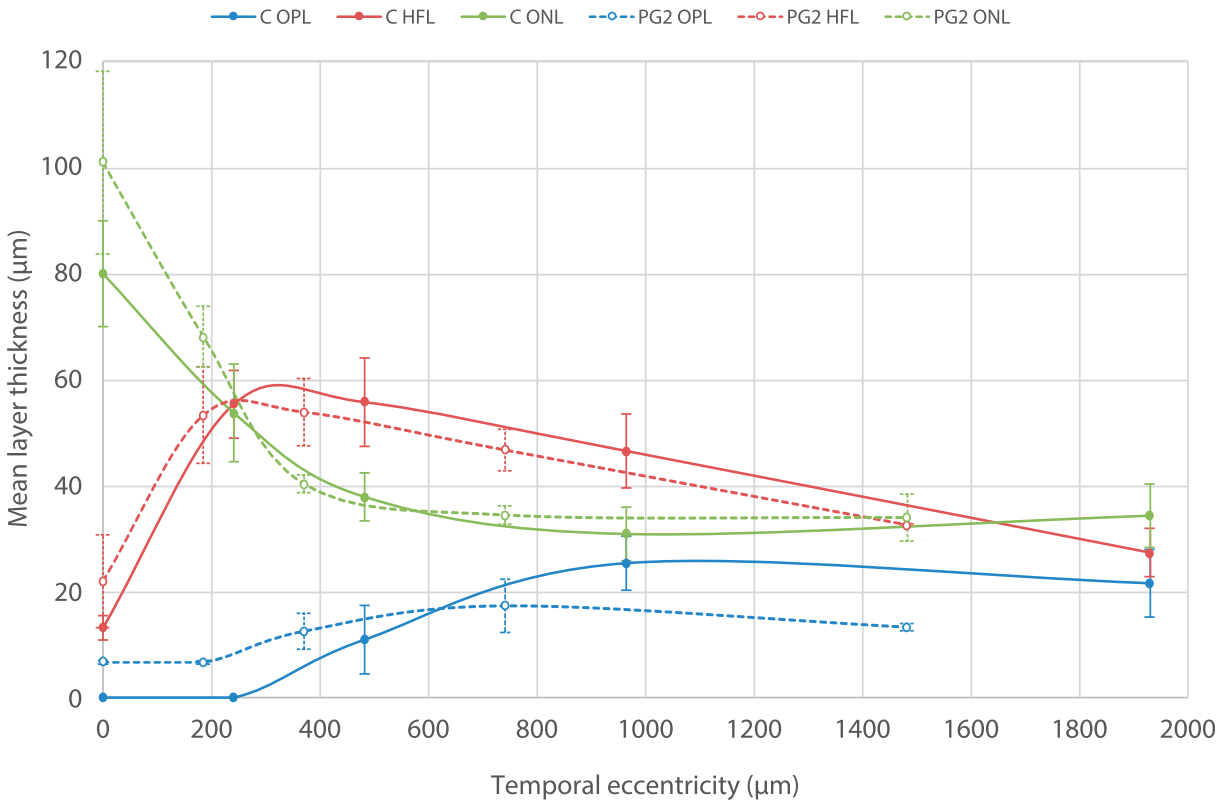

FIGURE 7. Manual segmentation data of OPL, HFL, and ONL thickness in micrometers (mean ± SD) along the temporal axis of control (C) and PG2 groups. The PG2 group shows increased central thickness of the ONL compared to controls as well as a central displacement of landmark positions. The PG2 group also shows a central OPL that is absent in the control group. Distance along temporal axis in micrometers.

thickness of the IRL below the ILM and a marked change in foveal contour. The lower part of the foveal slope out to 0.5R in controls is characterized by a steeper slope of the foveal contour. This region also contains the foveal capillary network encircling the foveal avascular zone.[37,38] The two selected measuring positions, 0.25R and 0.5R, are therefore placed in transition zones with marked changes in layer profiles. In controls, HFL reaches a maximal plateau at these positions, and at the 0.5R position the foveal slope is steepest and ONL reaches a basal level following a decline from its maximum at FC. The inclusion of two extra central measuring positions, 0.125R and 0.1875R, gave less information and was omitted in the analysis of tilted images.

The OPL covers the FC in preterms with arrested foveal development as has been shown by reflectometry during normal development.[10] This indicates that some cone pedicles and synapses are present in the central part of the fovea and require more vertically oriented Henle fibers to connect with corresponding central photoreceptor segments. Two cases of preterms without visible changes in foveal contour (PG1) show a decreased width of the OPL free central zone as noted in some preterm children born before 27 gestational weeks in our previous study of extreme prematurity.[26] A more central location of the OPL edge may be interpreted as a sign of immaturity representing an intermediate phase between incomplete and complete central IRL displacement. Furthermore, Tick and colleagues[6] suggest that the structural variability in normal subjects may correspond to variations of the size of the foveal avascular zone and foveal development.

The inter-OPL distance, that is, the distance between the edges of the OPL, seems to have relevance as a clinical parameter as shown by Kim and colleagues.[39,40] They used the inter-OPL distance in clinical studies of the foveal structure following macular hole surgery to define the asymmetric elongation of foveal tissue central to the OPL edge as a possible effect of decreased postoperative foveolar stability after ILM peeling. In a recent study by another group the inter-OPL distance of the fellow eye was used to adjust for macular hole diameter and morphologic variations assuming that eyes with larger foveolar floor have larger hole diameter.[41]

The foveal rim is defined by the position where the retina reaches its greatest total thickness and is the anatomic representation of the margin of the fovea.[16] Half the inter-rim distance constitutes the foveal radius. This landmark, characterized by maximal total retinal thickness and IRL thickness, was easily defined in OCT images of all cases but one that lacked a foveal depression (case PG3-2).

The standard definition of FC is traditionally the center of the foveal pit, and this normally coincides with the peak of the OS bulge. However, it has been shown that arrested development of premature retinas primarily affects the morphology of the IRL with little or no lateral changes in the outer retinal layers. Since the focus of this study was to describe changes of the outer retina, and in order to avoid changes caused by possible asymmetric changes of the IRL, we selected the position of the longitudinal reflectometric profile with the most well-defined peaks within ±3 pixels from the peak of the OS bulge maximum as the definition of FC.

The more central position of the foveal rim in the two PG with arrested foveal development (PG2 and PG3) corresponds to the observation by Yanni and colleagues[25] of a decreased foveal diameter in cases with ROP compared to controls and preterms without ROP. One possible explanation for the more central position of the foveal rim in the immature retina could be a reduced displacement of IRL structures in preterms with arrested foveal development.

Downloaded from iovs.arvojournals.org on 04/25/2024

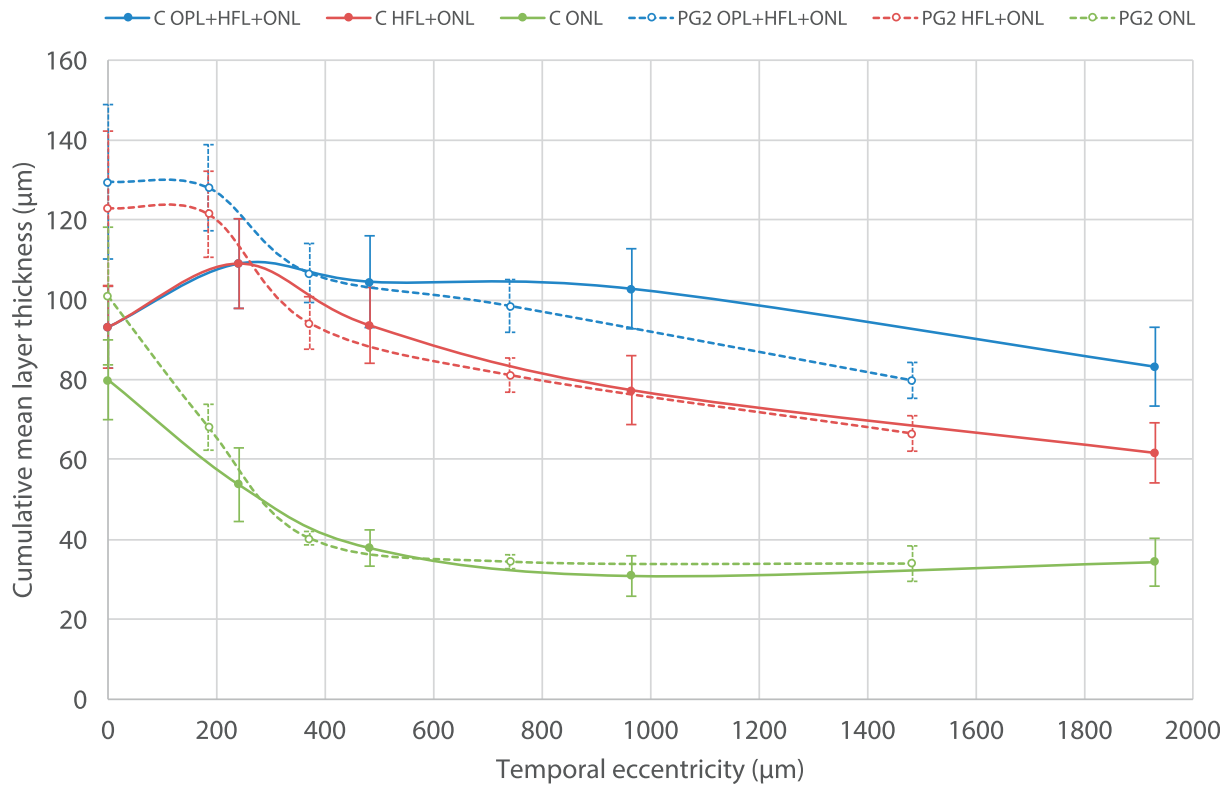

Figure 8. Cumulative layer thickness in micrometers (mean ± SD) from manual segmentation data of OPL + HFL + ONL, HFL + ONL, and ONL along temporal axis of control (C) and PG2 groups. The PG2 group shows increased central thickness of these layers compared to controls as well as a central displacement of landmark positions. Distance along temporal axis in micrometers.

Our FC/R landmark transformation adjusts for differences in foveal rim position and improves the ability of comparing interindividual B-scans.[4–6] The finding of a 20% shorter FC to R distance in preterms with an immature fovea than in controls makes the size adjustment even more important for discriminating deviations in premature retina from normal. Knighton and colleagues[42] have previously shown that foveal size correction reduces variance when mapping ganglion cell layers and likely improves the ability to discriminate abnormal maps. Measurements at defined landmark positions were used to facilitate comparisons between groups and we used two eccentricity scales based on foveal rim (R) positions for adjusted foveal size or an absolute scale of micrometers.

The profile and thickness of the combined OPL + HFL + ONL of these preterms seemed to be increased centrally compared to controls, in line with previous studies.[26–28] Directional OCT was needed to separate the true HFL from the true ONL as described in earlier studies.[12–14] The absolute and relative contributions of the OPL, HFL, and ONL to the thickening of the retina and reduced FD in arrested foveal development were described for the first time according to our knowledge.

This supernormal central increase of the combined thicknesses of the photoreceptor cell body (ONL) and pedicle/synapse layers (OPL) is remarkable since it does not fit into the timeline of normal development where a monotonic increase of the combined OPL + HFL + ONL is seen.[21,22] To explain our finding of an increased true ONL thickness in developmental arrest, our hypothesis is that the decreased displacement of retinal ganglion and bipolar cells decreases the centrifugal pull on the synaptically connected cone pedicles and photoreceptor cell bodies. A consequence of the retarded displacement of cone pedicles is that their axons have to be more vertically oriented within the foveola. The course of the normally oblique columns of ONL cell bodies[43] also changes to a more vertical direction, thereby increasing the height of the central ONL. An alternative explanation such as an increase in photoreceptor cell numbers is less probable since the ONL cell population seems to be unchanged after midgestation.[1] No prediction is made about the thickness of the HFL within the foveola in this hypothesis of decreased centrifugal pull within the central fovea, since the thickness of the HFL is a function of number, length, and angle of axons. We found only a marginal increase at FC for this layer in the present study, which may be an effect of more vertically oriented fibers at FC.

The photoreceptor inner and outer segment layers (IS/OS) could be well defined in the reflectometric profiles, and manual segmentation added little information. The three hyperreflective peaks (ELM, IS/OS, and IZ) corresponding to layers extending from the ELM to the IZ were all well defined in controls as well as in preterms in the present study. These peaks normally appear during the second postnatal year.[10] Vajzovic and colleagues[21] suggest that these reflective bands are fully mature at 13 to 15 years in their combined OCT and histologic study of human foveal maturation.

The profiles and thicknesses of separate OS and IS layers of preterms with arrested foveal development showed no observable change compared to controls as shown in a previous study.[27] This indication of structural normality of OS in these preterms contrasts to reports of absence of an OS bulge in some preterms with worse visual prognosis.[44] Signs of delayed maturation of the IS/OS or ellipsoid zone as described during early development of very preterm infants[45] were not observed in the present study by reflectometry at adult age.

Downloaded from iovs.arvojournals.org on 04/25/2024

Lacking clear evidence of changed photoreceptor segment structure, further studies are needed to provide insight about changes of other layers within the central fovea that may cause decreased mfERG responses[46–49] or retinal sensitivity[32] in some preterms. The observations in the present study of marked changes within the inner photoreceptor layers including the pedicle/synapse layer of the foveola, with limited space for the central pedicles due to decreased areal magnification from cone inner segments to cone pedicles[35,50] caused by reduced displacement, may be of importance to explain decreased central retinal function in preterms.

A foveal OS bulge was present in all images of preterms as described in a previous study.[26] Our analysis showed that this central OS bulge was caused by lengthening of the outer segments and not the inner segments. However, our attempt to quantitatively define the limits of the foveal OS bulge was unsuccessful. Although the slope of OS decline was most marked out to 200 μm in both controls and preterms, the slope continued peripherally without any definable landmark as noticed in normal subjects in a previous reflectometric study.[51]

The current study has limitations that must be taken into consideration in order to assess the significance of the results and conclusions. First, it was to some extent limited by the small number of subjects. The examinations were extremely demanding, requiring between 15 and 30 scans at one or two occasions in order to obtain enough high-quality images that captured the foveal reflex in different tilt positions. During the search for suitable subjects it was noticed that preterms with signs of foveal immaturity, more often than controls, lack the obvious sign of a clear foveal reflex as detected by OCT. They have more difficulties in keeping a strict fixation for a longer time period and more often have a displaced corneal apex, which causes difficulties in obtaining tilted scans with directional OCT. However, we believe that the final group of subjects, showing a clear foveal reflex and a range in signs of foveal immaturity, is representative of a larger group of preterms with comparable demographics.

Second, data collection was performed using semiautomated reflectivity analysis, even though there are freely available multilayer segmentation algorithms as well as a built-in segmentation algorithm in the Cirrus HD-OCT. However, to the best of our knowledge, these algorithms do not allow for individual segmentation of the HFL and ONL. In addition, eyes with incomplete extrusion of the IRL present difficulties for the built-in segmentation algorithm of the Cirrus HD-OCT, resulting in erroneous layer segmentation in the central fovea.[33]

In summary and in conclusion, the results of the present study suggest that analysis of anatomic features such as landmarks and thickness profiles of different retinal layers in preterms can demonstrate marked redistributions within cell populations in preterms with arrested foveal development. Our results extend previous observations by delineating the changes in separate layers of the outer part of the fovea. The present study shows a central thickness increase in layers consisting of photoreceptor cell bodies (ONL) and pedicles/synapses (OPL) in preterms with signs of arrested foveal development in addition to a thickness increase of postreceptor layers. The reduced FD may thus be caused to an equal or dominating part by thickening of the combined ONL and OPL compared to that of postreceptor layers. However, we were unable to show any change in IS or OS thickness in preterms.

Acknowledgments

Supported by the Göteborg Medical Society (14/410151), the De Blindas Vänner i Göteborg Foundation (79/15), and the Royal Society of Arts and Sciences in Gothenburg.

Disclosure: **J. Sjöstrand**, None; **R. Rosén**, None; **M. Nilsson**, None; **Z. Popovic**, None

References

1. Hendrickson AE. Primate foveal development: a microcosm of current questions in neurobiology. *Invest Ophthalmol Vis Sci*. 1994;35:3129–3133.
2. Provis JM, Dubis AM, Maddess T, Carroll J. Adaptation of the central retina for high acuity vision: cones, the fovea and the avascular zone. *Prog Retin Eye Res*. 2013;35:63–81.
3. ETDRS Research Group. Grading diabetic retinopathy from stereoscopic color fundus photographs–an extension of the modified Airlie House classification. ETDRS report number 10. *Ophthalmology*. 1991;98:786–806.
4. Dubis AM, Hansen BR, Cooper RF, Beringer J, Dubra A, Carroll J. Relationship between the foveal avascular zone and foveal pit morphology. *Invest Ophthalmol Vis Sci*. 2012;53:1628–1636.
5. Dubis AM, McAllister JT, Carroll J. Reconstructing foveal pit morphology from optical coherence tomography imaging. *Br J Ophthalmol*. 2009;93:1223–1227.
6. Tick S, Rossant F, Ghorbel I, et al. Foveal shape and structure in a normal population. *Invest Ophthalmol Vis Sci*. 2011;52:5105–5110.
7. Huang D, Swanson EA, Lin CP, et al. Optical coherence tomography. *Science*. 1991;254:1178–1181.
8. Rothman AL, Mangalesh S, Chen X, Toth CA. Optical coherence tomography of the preterm eye: from retinopathy of prematurity to brain development. *Eye Brain*. 2016;8:123–133.
9. Huang Y, Cideciyan AV, Papastergiou GI, et al. Relation of optical coherence tomography to microanatomy in normal and rd chickens. *Invest Ophthalmol Vis Sci*. 1998;39:2405–2416.
10. Dubis AM, Costakos DM, Subramaniam CD, et al. Evaluation of normal human foveal development using optical coherence tomography and histologic examination. *Arch Ophthalmol*. 2012;130:1291–1300.
11. McAllister JT, Dubis AM, Tait DM, et al. Arrested development: high-resolution imaging of foveal morphology in albinism. *Vision Res*. 2010;50:810–817.
12. Lujan BJ, Roorda A, Croskrey JA, et al. Directional optical coherence tomography provides accurate outer nuclear layer and Henle fiber layer measurements. *Retina*. 2015;35:1511–1520.
13. Lujan BJ, Roorda A, Knighton RW, Carroll J. Revealing Henle's fiber layer using spectral domain optical coherence tomography. *Invest Ophthalmol Vis Sci*. 2011;52:1486–1492.
14. Otani T, Yamaguchi Y, Kishi S. Improved visualization of Henle fiber layer by changing the measurement beam angle on optical coherence tomography. *Retina*. 2011;31:497–501.
15. Agarwal A. *Gass' Atlas of Macular Diseases*. 5th ed. China: Elsevier Saunders; 2011:1378.
16. Polyak SL. *The Retina; the Anatomy and the Histology of the Retina in Man, Ape, and Monkey, Including the Consideration of Visual Functions, the History of Physiological Optics, and the Histological Laboratory Technique*. Chicago, IL: The University of Chicago Press; 1941:607.
17. Curcio CA, Messinger JD, Sloan KR, Mitra A, McGwin G, Spaide RF. Human chorioretinal layer thicknesses measured in macula-wide, high-resolution histologic sections. *Invest Ophthalmol Vis Sci*. 2011;52:3943–3954.
18. Hendrickson A, Possin D, Vajzovic L, Toth CA. Histologic development of the human fovea from midgestation to maturity. *Am J Ophthalmol*. 2012;154:767–778.e2.

Downloaded from iovs.arvojournals.org on 04/25/2024

19. Hendrickson AE, Yuodelis C. The morphological development of the human fovea. *Ophthalmology*. 1984;91:603–612.
20. Yuodelis C, Hendrickson A. A qualitative and quantitative analysis of the human fovea during development. *Vision Res*. 1986;26:847–855.
21. Vajzovic L, Hendrickson AE, O'Connell RV, et al. Maturation of the human fovea: correlation of spectral-domain optical coherence tomography findings with histology. *Am J Ophthalmol*. 2012;154:779–789.e2.
22. Lee H, Purohit R, Patel A, et al. In vivo foveal development using optical coherence tomography. *Invest Ophthalmol Vis Sci*. 2015;56:4537–4545.
23. Sjöstrand J, Popovic Z. A time-line model of developmental events within the human fovea based on imaging and histology. *Acta Ophthalmol*. 2013;91:S100.
24. Maldonado RS, O'Connell RV, Sarin N, et al. Dynamics of human foveal development after premature birth. *Ophthalmology*. 2011;118:2315–2325.
25. Yanni SE, Wang J, Chan M, et al. Foveal avascular zone and foveal pit formation after preterm birth. *Br J Ophthalmol*. 2012;96:961–966.
26. Rosén R, Sjöstrand J, Nilsson M, Hellgren K. A methodological approach for evaluation of foveal immaturity after extremely preterm birth. *Ophthalmic Physiol Opt*. 2015;35:433–441.
27. Hammer DX, Iftimia NV, Ferguson RD, et al. Foveal fine structure in retinopathy of prematurity: an adaptive optics Fourier domain optical coherence tomography study. *Invest Ophthalmol Vis Sci*. 2008;49:2061–2070.
28. Wang J, Spencer R, Leffler JN, Birch EE. Critical period for foveal fine structure in children with regressed retinopathy of prematurity. *Retina*. 2012;32:330–339.
29. Schindelin J, Arganda-Carreras I, Frise E, et al. Fiji: an open-source platform for biological-image analysis. *Nat Methods*. 2012;9:676–682.
30. Bennett AG, Rudnicka AR, Edgar DF. Improvements on Littmann's method of determining the size of retinal features by fundus photography. *Graefes Arch Clin Exp Ophthalmol*. 1994;232:361–367.
31. Putnam NM, Hammer DX, Zhang Y, Merino D, Roorda A. Modeling the foveal cone mosaic imaged with adaptive optics scanning laser ophthalmoscopy. *Opt Express*. 2010;18:24902–24916.
32. Bowl W, Stieger K, Bokun M, et al. OCT-based macular structure-function correlation in dependence on birth weight and gestational age – the Giessen Long-Term ROP Study. *Invest Ophthalmol Vis Sci*. 2016;57:OCT235–OCT241.
33. Nilsson M, Hellstrom A, Jacobson L. Retinal sequelae in adults treated with cryotherapy for retinopathy of prematurity. *Invest Ophthalmol Vis Sci*. 2016;57:OCT550–OCT555.
34. Provis JM, Penfold PL, Cornish EE, Sandercoe TM, Madigan MC. Anatomy and development of the macula: specialisation and the vulnerability to macular degeneration. *Clin Exp Optom*. 2005;88:269–281.
35. Missotten L. Estimation of the ratio of cones to neurons in the fovea of the human retina. *Invest Ophthalmol*. 1974;13:1045–1049.
36. Yamada E. Some structural features of the fovea centralis in the human retina. *Arch Ophthalmol*. 1969;82:151–159.
37. Chui TY, VanNasdale DA, Elsner AE, Burns SA. The association between the foveal avascular zone and retinal thickness. *Invest Ophthalmol Vis Sci*. 2014;55:6870–6877.
38. Popovic Z, Knutsson P, Thaung J, Owner-Petersen M, Sjostrand J. Noninvasive imaging of human foveal capillary network using dual-conjugate adaptive optics. *Invest Ophthalmol Vis Sci*. 2011;52:2649–2655.
39. Kim JH, Kang SW, Lee EJ, Kim J, Kim SJ, Ahn J. Temporal changes in foveal contour after macular hole surgery. *Eye (Lond)*. 2014;28:1355–1363.
40. Kim JH, Kang SW, Park DY, Kim SJ, Ha HS. Asymmetric elongation of foveal tissue after macular hole surgery and its impact on metamorphopsia. *Ophthalmology*. 2012;119:2133–2140.
41. Shin JY, Chu YK, Hong YT, Kwon OW, Byeon SH. Determination of macular hole size in relation to individual variabilities of fovea morphology. *Eye (Lond)*. 2015;29:1051–1059.
42. Knighton RW, Gregori G, Budenz DL. Variance reduction in a dataset of normal macular ganglion cell plus inner plexiform layer thickness maps with application to glaucoma diagnosis. *Invest Ophthalmol Vis Sci*. 2012;53:3653–3661.
43. Ahnelt PK, Schubert C, Anger EM. Macular photoreceptor organization. In: Binder S, ed. *The Macula: Diagnosis, Treatment and Future Trends*. Vienna: Springer; 2012:1–7.
44. Villegas VM, Capo H, Cavuoto K, McKeown CA, Berrocal AM. Foveal structure-function correlation in children with history of retinopathy of prematurity. *Am J Ophthalmol*. 2014;158:508–512, e502.
45. Vajzovic L, Rothman AL, Tran-Viet D, Cabrera MT, Freedman SF, Toth CA. Delay in retinal photoreceptor development in very preterm compared to term infants. *Invest Ophthalmol Vis Sci*. 2015;56:908–913.
46. Akerblom H, Andreasson S, Holmstrom G. Macular function in preterm children at school age. *Doc Ophthalmol*. 2016;133:151–157.
47. Altschwager P, Moskowitz A, Fulton AB, Hansen RM. Multifocal ERG responses in subjects with a history of preterm birth. *Invest Ophthalmol Vis Sci*. 2017;58:2603–2608.
48. Fulton AB, Hansen RM, Moskowitz A, Barnaby AM. Multifocal ERG in subjects with a history of retinopathy of prematurity. *Doc Ophthalmol*. 2005;111:7–13.
49. Michalczuk M, Urban B, Chrzanowska-Grenda B, Ozieblo-Kupczyk M, Bakunowicz-Lazarczyk A, Kretowska M. The assessment of multifocal ERG responses in school-age children with history of prematurity. *Doc Ophthalmol*. 2016;132:47–55.
50. Ahmad KM, Klug K, Herr S, Sterling P, Schein S. Cell density ratios in a foveal patch in macaque retina. *Vis Neurosci*. 2003;20:189–209.
51. Kay DB, Land ME, Cooper RF, et al. Outer retinal structure in best vitelliform macular dystrophy. *JAMA Ophthalmol*. 2013;131:1207–1215.

Investigative Ophthalmology & Visual Science

Downloaded from iovs.arvojournals.org on 04/25/2024